*Biochimica et Biophysica Acta*, 1062 (1991) 211–219

*ADONIS* 000527369100118M

BBAMEM 75136



# Structure and thermotropic properties of hydrated *N*-stearoyl sphingomyelin bilayer membranes

P.R. Maulik, P.K. Sripada and G.G. Shipley

*Departments of Biophysics and Biochemistry, Housman Medical Research Center, Boston University School of Medicine, Boston, MA (U.S.A.)*

(Received 25 April 1990)
(Revised manuscript received 3 October 1990)

Key words: Sphingomyelin; Lipid bilayer; Thermodynamics; X-ray diffraction; DSC

**Hydrated multibilayers of *N*-stearoyl sphingomyelin were investigated as a function of hydration using differential scanning calorimetry (DSC) and X-ray diffraction. Anhydrous *N*-stearoyl sphingomyelin exhibits an endothermic transition at 75 °C ($\Delta H = 3.8$ kcal/mol); increasing hydration progressively lowers the transition temperature and increases the transition enthalpy, until limiting values ($T_m = 45$ °C, $\Delta H = 6.7$ kcal/mol) are observed for hydration values > 21.4% $H_2O$. At low hydration levels, < 20% $H_2O$, an additional transition is observed at approx. 20 °C. X-ray diffraction studies at temperatures below (22 °C) and above (55 °C) the main endothermic transition confirm that the bilayer gel (sharp 4.2 Å reflection) → bilayer liquid crystal (diffuse 4.5 Å reflection) transition occurs at all hydration levels with limiting bilayer hydration occurring at approx. 31.5% $H_2O$ in the gel phase and at approx. 35% $H_2O$ in the liquid crystal phase. The thermotropic properties and metastability of this partial synthetic *N*-stearoyl sphingomyelin differ in some respects from that of the previously studied synthetic DL-*erythro*-*N*-stearoyl sphingomyelin (Estep, T.N., Calhoun, W.I., Barenholz, Y., Biltonen, R.L., Shipley, G.G. and Thompson, T.E. (1980) Biochemistry 19, 20–24), suggesting an influential role of the interfacial molecular conformation.**

## Introduction

The lipid bilayer matrix of plasma membranes is comprised of specific molecular blends of glycerophospholipids, sphingolipids and cholesterol. The more polar glycerophospholipids (e.g., phosphatidylcholine, phosphatidylethanolamine, phosphatidylserine) and sphingolipids (e.g., sphingomyelin, cerebroside) readily form the lipid bilayer compartment in which cholesterol is soluble and in which membrane proteins are incorporated with a specific molecular orientation. The orientation of membrene proteins is such that they can efficiently fulfill receptor, signaling and transport functions. In addition, the lipid bilayer itself appears to maintain an asymmetric disposition with respect to its polar lipid constituents. For example, the red cell membrane has a preferential location of the two choline-containing phospholipids, phosphatidylcholine (PC) and sphingomyelin (SM) in its external monolayer and glycosphingolipids appear to reside exclusively in the external monolayer. Furthermore, the two polar lipids PC and SM are the dominant polar lipids present on the surface monolayer of the fat-transporting serum lipoproteins. Together with proteins, SM and PC are the polar lipids primarily responsible for the overall stability of the spherical cholesterol ester- and acylglycerol-containing lipoprotein particles in aqueous media.

In contrast to glycerophospholipids in general and PC in particular, relatively little information is available on the physical properties of SM (for reviews, see Refs. 1 and 2). Early monolayer studies by Shah and Schulman [3,4] showed that bovine heart SM exhibited a limiting surface area of 42–43 $Å^2$, a value similar to that of dipalmitoyl PC. Reiss-Husson [5] showed that hydrated bovine brain SM formed bilayers at 40 °C. Our initial X-ray diffraction and differential scanning calorimetry (DSC) study of bovine brain SM [6] showed that its bilayer gel → liquid crystal transition occurred at a surprisingly high temperature for a naturally occurring lipid (30–40 °C). Similar behavior was observed by Barenholz et al. [7] in their study of bovine brain SM.

Correspondence to: G.G. Shipley, Departments of Biophysics and Biochemistry, Housman Medical Research Center, Boston University School of Medicine, Boston, MA 02118-2394, U.S.A.

These studies of bovine brain SM preceded our studies of its interaction with cholesterol (Avecilla, L.S. and Shipley, G.G., unpublished observations) and egg yolk PC [8]; note also the prior studies of SM–cholesterol interactions by DSC and NMR [9], ESR [10] and X-ray diffraction [11].

The interpretation of the studies with bovine brain SM are complicated by the chemical heterogeneity of the amide-linked fatty acid (see, for example, Ref. 12) and, to a lesser extent, the sphingosine moiety. This has led to attempts to synthesize SM with specific amide-linked fatty acid chains either by de novo synthesis [13] or by partial synthesis starting with bovine brain SM [14–16]. A calorimetric study of C16:0-, C18:0- and C24:0-SM synthesized with the sphingosine in the DL-*erythro* configuration showed an interesting pattern of behavior [7]. While hydrated C16:0-SM showed a simple, reversible gel → liquid crystal transition at approx. 41°C, the longer chain C18:0- and C24:0-SM exhibited additional exothermic and endothermic transitions. The complex behavior of DL-*erythro* C18:0-SM was subsequently investigated and two low temperature bilayer forms were identified: a *stable* bilayer phase which melts at 57°C, $\Delta H = 20$ kcal/mol, and a *metastable* bilayer phase melting at 44°C, $\Delta H = 7$ kcal/mol [17]. The interaction of these DL-*erythro*-SM with cholesterol was also studied by calorimetric methods [18,19].

Our own studies focused initially on the partial synthesis of C16:0-SM by deacylation and reacylation of bovine brain SM, followed by a study of its structure and interactions with PC and cholesterol [14]. X-ray diffraction and DSC studies showed that C16:0-SM exhibits a reversible bilayer gel → bilayer liquid crystal transition at 40.5°C ($\Delta H = 5.8$ kcal/mol), the bilayer repeat distance being 66.8 Å at 10°C and 61.6 Å at 50°C [14]. In addition, C16:0-SM and dimyristoyl PC were shown to be miscible in both the gel and liquid crystal phases (see also Ref. 20). In contrast to immiscible SM-PC systems where cholesterol appears to have higher affinity for SM [21], no preferential affinity for either SM or PC was found in the miscible system [14].

Recently, we have extended our partial synthesis of SM to include C14:0-, C16:0-, C18:0-, C20:0-, C22:0-, C24:0- and C24:1-SM and initial calorimetric studies show, in contrast to the diacyl-PC series, a complex pattern of thermotropic behavior [22]. In particular, the short chain (C14:0) and long chain (C22:0 and C24:0) SM exhibit complex thermotropic behavior, presumably due to a mismatch in the length of the *N*-acyl chain compared to the sphingosine chain. We have also shown by X-ray scattering that single bilayer vesicles made from this series of SM show an unusual dependence of the bilayer thickness with chain length, again presumably as a consequence of different chain packing arrangements across the bilayer center [23]. In this paper we describe the structure and thermotropic properties of hydrated C18:0-SM as revealed by X-ray diffraction and scanning calorimetry.

## Materials and Methods

### *Synthesis of C18:0-SM*

Details of the partial synthesis of C18:0-SM from bovine brain SM are given in Ref. 22. Briefly, 2 g of bovine brain SM (Calbiochem, La Jolla, CA) with heterogeneous *N*-acyl chains were subjected to acid hydrolysis [24] and sphingosylphosphorylcholine (SPC) was isolated using silicic acid column chromatography in a yield of 35% (530–560 mg). SPC was then acylated using stearoylimidazolide and the product *O*-*N*-distearoyl SPC (≈ 450 mg) isolated using column chromatography. The *O*-*N*-distearoyl SPC was then treated under mild alkaline conditions to hydrolyze the *O*-ester bond. C18:0-SM (210 mg) was isolated using silicic acid column chromatography. The resulting C18:0-SM was vacuum dried at approx. 75°C and routine analytical IR studies showed no evidence of residual hydration in the sample (data not shown). C18:0-SM was shown to be chromatographically pure (> 99%) by a combination of thin-layer chromatography and high performance liquid chromatography (see Ref. 22 for details and other synthetic strategies). A problem associated with the synthesis of C18:0-SM from naturally occurring D-*erythro* bovine brain SM via the deacylation-reacylation pathway concerns inversion at C-3 during acid hydrolysis, as described in detail in one of our previous studies [22]. Due to this epimerization at C-3 as revealed by $^{13}$C-NMR and specific rotation studies, a significant amount of the L-*threo* stereoisomer of SPC was formed, hence the resulting SM consisted of a mixture of D-*erythro* and L-*threo* sphingomyelins. So far we have not been able to separate the D-*erythro* and L-*threo* isomers of SPC using column chromatography and preparative TLC. The extent of epimerization varied between preparations but in all cases significant amounts of the L-*threo* isomer were present, particularly when the method of Kaller [24] was used (see detailed study of C16:0-SM in Ref. 22).

The sphingosine base compositions of bovine brain SM and C16:0-SM were determined by HPLC (see Ref. 22). A similar base composition dominated by C18:1*t* would be expected for C18:0-SM.

### *Differential scanning calorimetry*

For calorimetric studies, samples were weighed into stainless steel pans and the calculated amount of doubly distilled water was added to the dry sample using a microsyringe to give various hydration states of C18:0-SM. The sample pans were hermetically sealed and placed in a Perkin-Elmer DSC-2 differential scanning calorimeter (Norwalk, CT) to perform heating and cool-

ing scans. Each sample was heated and cooled repeatedly at a rate of 5 C°/min in the range between 0 and 80°C. The peak in the heat capacity vs. temperature plot was recorded as the transition temperature, $T_m$ (estimated error, ±0.2 C°); the transition enthalpies, $\Delta H$ (estimated error, ±0.2 kcal/mol) were determined from the areas under the transition endotherm peak as measured by planimetry and compared with the known enthalpy of a standard (gallium).

*X-ray diffraction*

Samples of anhydrous C18:0-SM were weighed directly into quartz capillaries (internal diameter = 1.0 mm). Appropriate amounts of doubly distilled water were added by microsyringe and the capillary tubes were flame-sealed immediately. The capillaries were centrifuged several times at temperatures 10 C° above the phase transition temperature to achieve equilibration of the multilamellar lipid/water systems.

The X-ray diffraction patterns were recorded using focussing cameras with either toroidal mirror [25], or double mirror [26] optics, and photographic detection. Nickel-filtered Cu$K_\alpha$ ($\lambda = 1.5418$ Å) radiation was obtained from an Elliot GX6 rotating anode generator (Elliot Automation, Borehamwood, U.K.). The X-ray diffraction patterns were recorded at 22°C and 55°C, as well as other temperatures for samples at low hydration. Bilayer periodicities, $d$ (estimated error, ±0.9 Å) at each hydration were calculated from the lamellar reflections. The diffraction intensities were obtained using a Joyce-Loebl (Gateshead, U.K.) Model IIICS scanning microdensitometer.

For counter recording, Cu$K_\alpha$ X-radiation from amicrofocus X-ray generator (Jarrell-Ash, Waltham, MA) was line focused (100 μm × 14 mm) by a single mirror and collimated with the slit optical system of a Luzzati-Baro camera ($E^{TS}$ Beaudouin, Paris). X-ray diffraction data were recorded using a linear position sensitive detector (Tennelec, Oak Ridge, TN) and associated electronics (Tracor Northern, Middleton, WI).

## Results

*Differential scanning calorimetry*

Fig. 1 shows DSC heating/cooling scans of fully hydrated C18:0-SM (56.1 wt% water) following overnight (16 h) incubation at −4°C. The initial heating scan over the temperature range 0–77°C (Fig. 1a) shows a single sharp endothermic transition at 45°C ($\Delta H = 6.8$ kcal/mol C18:0-SM). The cooling scan (Fig. 1b) recorded immediately after the initial heating scan also shows a single transition exotherm at 43°C ($\Delta H = 6.9$ kcal/mol). Immediate reheating (Fig. 1c) shows the same behavior as that observed in the initial heating scan (cf. Fig. 1a). The transition onsets on heating and cooling both occur at approx. 44°C indicating that this

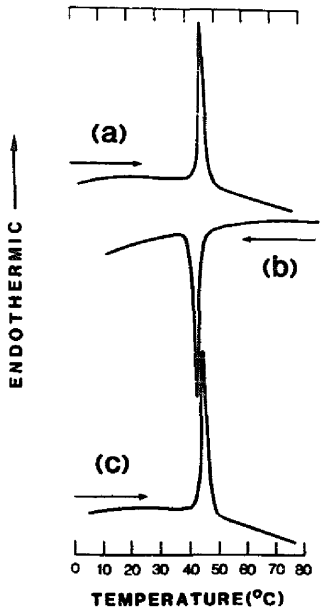


Fig. 1. DSC of fully hydrated (56.1 wt% $H_2O$) C18:0-SM. (a) Initial heating scan following overnight (16 h) incubation at −4°C. (b) Cooling scan immediately following (a). (c) Heating scan immediately following (b). Heating/cooling rates: 5 C°/min.

transition is reversible; at least at high hydrations and under these equilibration conditions, no low-temperature metastability is observed.

Fig. 2 shows representative DSC heating scans corresponding to the second heating run (see Fig. 1c for an example) of C18:0-SM at different hydration levels. In the absence of water, C18:0-SM exhibits a broad endothermic transition at 75°C ($\Delta H = 3.8$ kcal/mol). As the hydration increases, the transition temperature, $T_m$, decreases progressively and the transition enthalpy increases (see Table I), reaching limiting values, $T_m = 45$°C and $\Delta H = 6.7$ kcal/mol, at hydration levels $> \approx 25$ wt% $H_2O$. A plot of transition temperature ($T_m$) and transition enthapy ($\Delta H$) of C18:0-SM is shown as a function of water content in Fig. 3. At low hydration levels, < 20% $H_2O$), an additional transition is observed at approx. 20°C. The enthalpy associated with this transition is small ($\Delta H \cong 0.5$ kcal/mol) but increases with incubation time at −4°C. For example, C18:0-SM at 21.4% water exhibits no low-temperature transition on immediate reheating (see Fig. 2); however, 16 h incubation at −4°C produces a small but discernible transition at approx. 18°C ($\Delta H \cong 0.6$ kcal/mol) which after longer incubation times increases in transition enthalpy ($\Delta H \cong 1.6$ kcal/mol after 20 days at −4°C; data not shown).

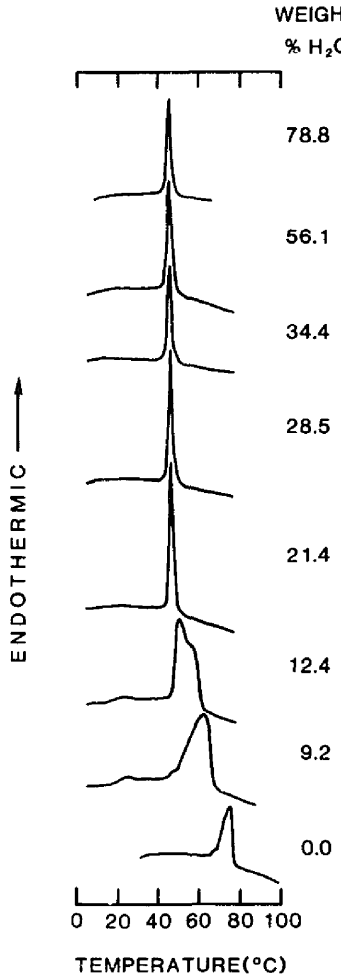


Fig. 2. Representative DSC heating scans of C18:0-SM at different hydration levels (range, 0.0 to 78.8 wt% water). The heating scans immediately following cooling from the $L_\alpha$ phase (see text) are shown. Heating rate: 5 C°/min.

Thus, although highly hydrated C18:0-SM exhibits essentially reversible thermotropic behavior, low temperature metastability and gel phase polymorphism are indicated at lower hydrations.

*X-ray diffraction*

X-ray diffraction data were recorded at 22°C and 55°C from hydrated (10–60 wt% $H_2O$) C18:0-SM. At low water contents (< 15 wt% $H_2O$), diffraction patterns were also recorded at 72°C. An example of the X-ray diffraction patterns of C18:0-SM (20 wt% $H_2O$) observed at temperatures below (22°C) and above

TABLE I

*DSC data of hydrated C18:0-SM*

| Wt% $H_2O$ | $T_m$(°C) | $\Delta H$ (kcal/mol) |
|---|---|---|
| 0.0 | 75.0 | 3.8 |
| 9.2 | 62.2 | 5.4 |
| 12.4 | 49.9 | 6.3 |
| 21.4 | 46.1 | 6.4 |
| 28.5 | 46.0 | 7.1 |
| 34.4 | 45.1 | 6.7 |
| 48.6 | 45.5 | 6.3 |
| 56.1 | 45.0 | 6.8 |
| 69.0 | 45.1 | 6.9 |
| 78.8 | 45.1 | 6.5 |

(55°C) the phase transition is shown in Fig. 4. At 22°C, a series of lamellar low-angle diffraction lines ($h = 1 \rightarrow 4$), bilayer periodicity, $d = 65.7$ Å, together with a sharp wide-angle reflection at 1/4.2 Å is observed. This X-ray diffraction pattern is typical of that observed for hydrated phospholipid bilayers in the gel phase with hexagonal chain packing. At 55°C, a series of lamellar low-angle diffraction lines ($h = 1 \rightarrow 4$) is again observed but corresponding to a reduced bilayer periodicity, $d = 57.9$ Å. In addition the broad, diffuse diffraction line at 1/4.5 $Å^{-1}$ is characteristic of the melted chain, liquid crystal phase. Similar lamellar X-ray diffraction patterns were recorded for C18:0-SM at other hydration levels (see below).

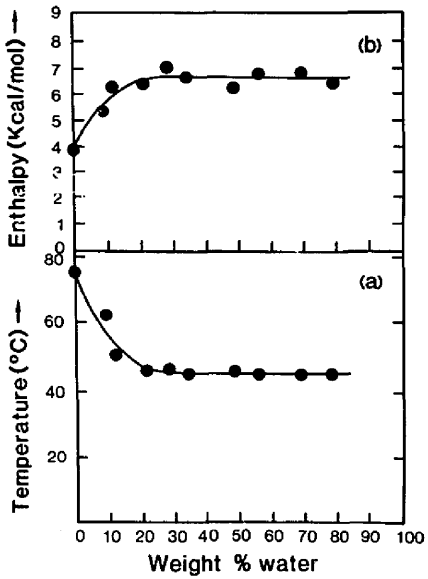


Fig. 3. Transition temperature (a) and transition enthalpy (b) of C18:0-SM as a function of hydration (wt% water).

A detailed study of the temperature dependence of the diffraction pattern of hydrated C18 : 0-SM (30 wt% $H_2O$) was made using the position sensitive detector (Fig. 5). Using a sample → detector distance = 104.2 mm, the diffraction pattern including the lamellar reflections $h = 2 \rightarrow 4$ (the first order reflection is obscured by the back-stop) and the wide-angle region ($1/2 \rightarrow 1/10$ Å$^{-1}$) is recorded at temperature increments of 4°C over the temperature range 12 to 68°C (Fig. 5, left). The low angle region was recorded with a sample → detector distance = 407.6 mm showing the behavior of the low-angle reflections $h = 1 \rightarrow 3$ (Fig. 5, right). At low temperatures the bilayer periodicity $d = 72.8$ Å and a sharp symmetrical wide-angle reflection at 1/4.17 Å$^{-1}$ is observed. In the temperature range 12 to 40°C, the bilayer periodicity decreases slightly from 72.8 to 70.1 Å, while the position of the wide angle reflection shifts from 1/4.17 to 1/4.26 Å$^{-1}$. At approx. 44°C, there are clear changes in both the positions and intensity distribution of the low and wide-angle reflections (see Fig. 5). At 48–49°C the bilayer periodicity is reduced to 69.4 Å and the wide-angle reflection has shifted to 1/4.53 Å$^{-1}$ and broadened significantly. With further increases in temperature, the bilayer periodicity decreases reaching a value of 62.2 Å at 58°C, whereas the wide angle reflection shows only a small shift in position (Fig. 5). These changes in both the low-angle and wide-angle reflections have been shown to be reversible on cooling (data not shown).

The bilayer periodicity, $d$, at 22°C and 55°C is plotted as a function of water content in Figs. 6a and b, respectively. At 22°C, C18 : 0-SM bilayers swell over the hydration range 10 to 32 wt% $H_2O$, the bilayer periodicity increasing from 62.5 to 74 Å. No further change in the bilayer periodicity is observed at > 32 wt% $H_2O$, thus defining the hydration limit of the gel phase of C18 : 0-SM. At 55°C, C18 : 0-SM containing 10 wt% $H_2O$ is in the bilayer gel phase. At 15 wt% $H_2O$ two bilayer periodicities are observed, suggesting that the bilayer gel and liquid crystal phases co-exist under these conditions. Over the hydration range 15 to 35 wt% $H_2O$, the liquid crystal bilayer phase of C18 : 0-SM exhibits bilayer swelling, $d$ increasing from approx. 56 Å to 66.6 Å. For water contents > 35 wt% $H_2O$, no further swelling is observed. For low water contents, X-ray diffraction data were also recorded at 72°C (i.e., in the melted chain, liquid crystal phase; see Fig. 2), the bilayer periodicities agreeing with the extrapolated periodicity data at 55°C (see Fig. 6b).

From the X-ray diffraction data, the structural parameters, $d_1$, the bilayer thickness, and $S$, the mean molecular surface area of the SM molecule at the lipid/

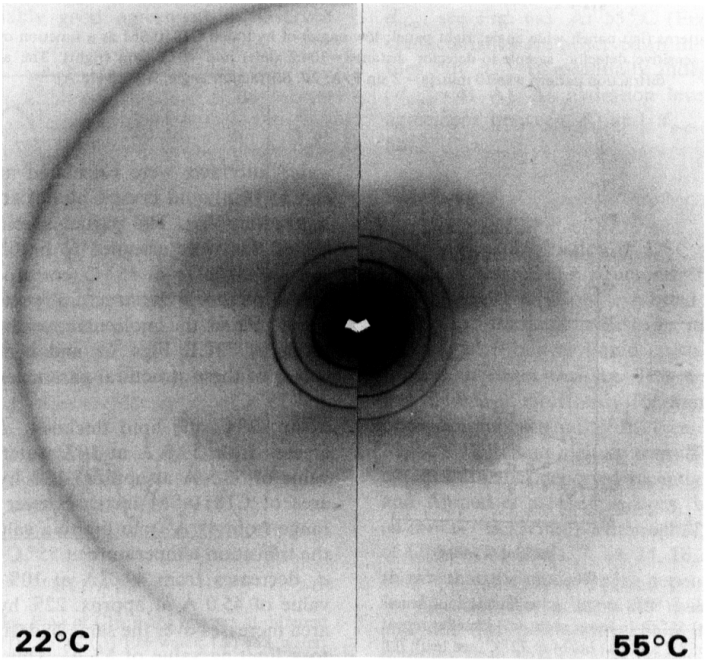


Fig. 4. X-ray diffraction patterns of C18 : 0-SM (20 wt% water) at 22°C (left) and 55°C (right). The diffraction patterns were recorded using double-mirror focusing optics (sample to film distance = 193.0 mm).

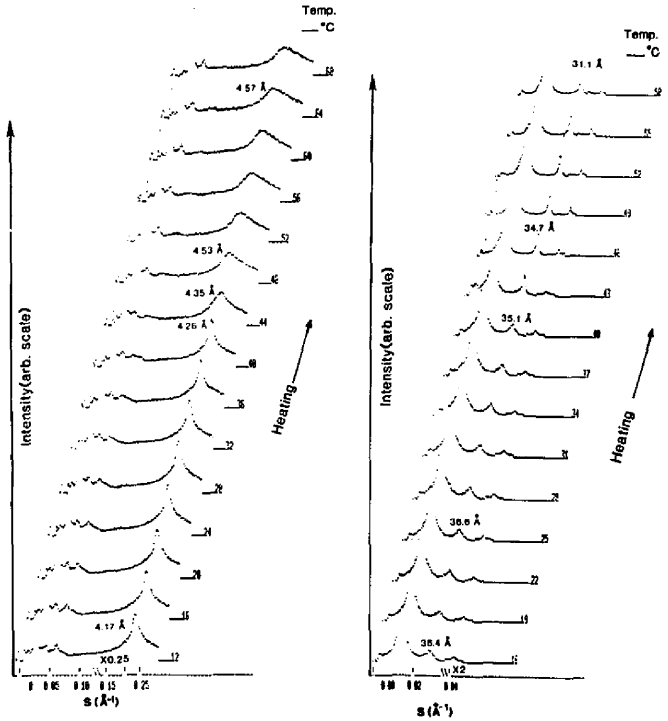


Fig. 5. X-ray diffraction patterns (left panel: wide angle; right panel: low angle) of hydrated C18:0-SM as a function of temperature. Data were recorded using a position-sensitive detector, sample-to-detector distance = 104.2 (left) and 407.6 mm (right). The acquisition time for each diffraction pattern was 10 min. [$s = 2 \sin\theta/\lambda$; $2\theta$, diffraction angle; $\lambda = 1.5418$ Å].

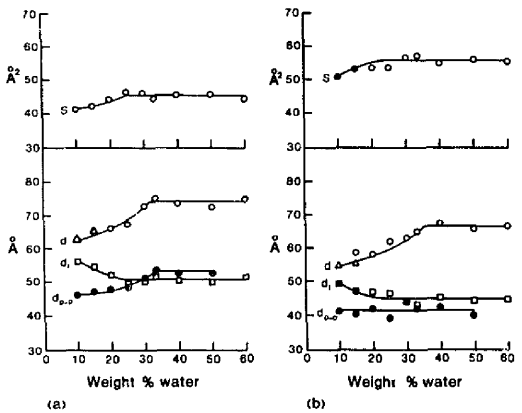


Fig. 6. Bilayer parameters of C18:0-SM as a function of water content at (a) 22°C and (b) 55°C. In lower plots, (○) lamellar repeat distance, $d$ [(Δ) in (a) at 55°C and (Δ) in (b) at 72°C, see text]; (□) lipid thickness, $d_1$ [(■) in (b) at 72°C]; (●) phosphate-phosphate distance, $d_{p\text{-}p}$. In upper plots, (○) surface area per C18:0-SM molecule at the lipid/water interface, $S$[(●) in (b) at 72°C, see text].

water interface, were calculated at 22°C (gel phase), and 55°C (liquid crystal phase) at different lipid concentrations [27]. The partial specific volumes ($v_1$) for C18:0-SM were assumed to be 0.9398 ml/g at 22°C and 1.0099 ml/g at 55°C (corresponding to values for similar phases of the structurally-related dipalmitoyl-PC, Ref. 28) and the molecular weight of C18:0-SM was taken as 731.1. Figs. 6a and b shows the calculated values of these structural parameters $d_1$ and $S$ at 22°C and 55°C.

At 22°C, the lipid thickness $d_1$ of C18:0-SM decreases from 59.8 Å at 10% water to reach a limiting value of 50.5 Å at approx. 25% hydration; the surface area of C18:0-SM increases over the same hydration range from 41 Å$^2$ to a limiting value of 45.0 Å$^2$. Above the transition temperature at 55°C (or 72°C, see above) $d_1$ decreases from 49.0 Å at 10% water to a limiting value of 45.0 Å at approx. 22% hydration; the surface area increases over the same hydration range from 51 Å$^2$ to a limiting value of 55 Å$^2$. Thus, as usual, the chain melting transition of, for example, fully hydrated C18:0-SM is accompanied by a decrease in bilayer

thickness, $d_l$, from 50.5 to 45 Å and an increase in the interfacial surface area from 45 to 55 Å$^2$ per C18 : 0-SM molecule.

In order to define further the C18 : 0-SM bilayer structure, electron density profiles accross the SM bilayer at different hydrations have been calculated using standard methods (see, for example, Refs. 29–34). The intensities of the lamellar low angle reflections have been corrected, scaled and converted to structure amplitudes $F(s)$ [35]. The plotted structure amplitudes trace out the continuous diffraction curve of a single bilayer and the nodes can be used to identify where the sign of the amplitude curve changes (Fig. 7). The continuous curves are calculated using the Shannon sampling theorem [36,37] (for details of our approach, see Ref. 34). At both 22 and 55 °C, the phase sequence 0, $\pi$, 0, $\pi$ was deduced (see Figs. 7a and b) and electron density profiles calculated according to these phases are shown in Fig. 8. At 22 °C (Fig. 8a) the centrosymmetric profiles all show a pronounced trough corresponding to the bilayer center ($X = 0$ Å) and two symmetry related peaks at greater than ±20 Å. These two peaks are due to the electron-rich phosphate groups of the polar moiety of C18 : 0-SM and their separation $d_{p\text{-}p}$ provides a measure of the bilayer thickness. Inspection of Fig. 8a shows that $d_{p\text{-}p}$ increases with increasing hydration (in contrast to the presumably related $d_l$ which decreases with increasing hydration) up to the hydration limit, at which point reasonably good agreement is observed between $d_l$ and $d_{p\text{-}p}$ (for a direct comparison of $d_l$ and $d_{p\text{-}p}$, see Fig. 6a). At 55 °C (Fig. 8b), similar bilayer characteristics are observed in the electron density profiles but $d_{p\text{-}p}$ is essentially independent of hydration ($d_{p\text{-}p} = 41$ Å). At hydration levels > 20% reasonable agreement between $d_l$ and $d_{p\text{-}p}$ is observed (see Fig. 6b).

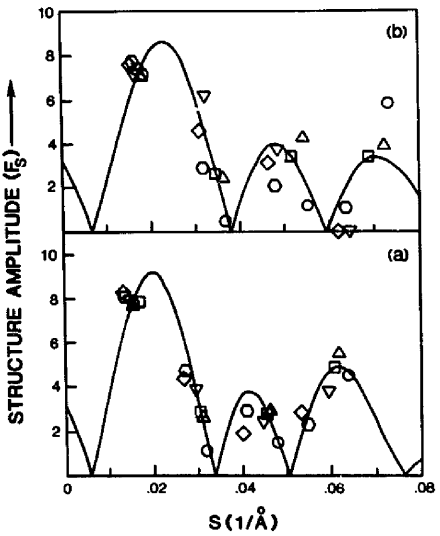


Fig. 7. Structure amplitudes $F(S)$ of C18 : 0-SM bilayers at different hydrations (a) 22 °C, and (b) 55 °C. (○) 10% water; (△) 15% water; (□) 20% water; (▽) 25% water; (○) 30% water; (◇) 33% water. The solid curves are derived by application of the Shannon sampling theorem (see Ref. 36) for the data of C18 : 0-SM/20% water.

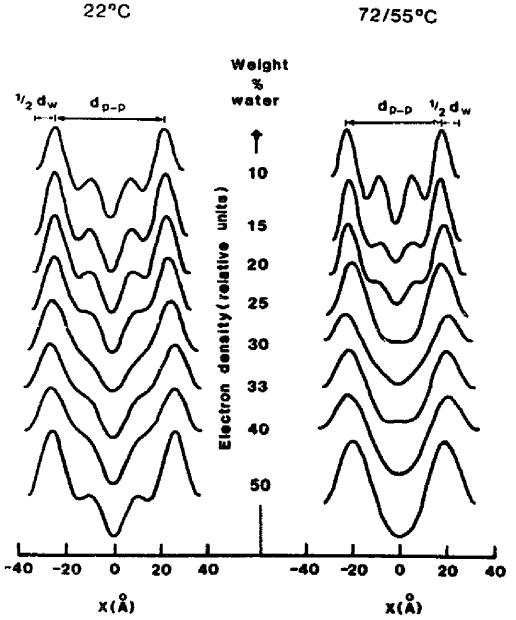


Fig. 8. Electron density profiles for C18 : 0-SM at different hydrations: 22 °C (left) and 55(72) °C (right).

## Discussion

Using a combination of DSC and X-ray diffraction we have defined the structural changes accompanying the thermal transitions exhibited by hydrated C18 : 0-SM. The reversible transition at 45 °C is due to a bilayer gel → bilayer liquid crystal associated with hydrocarbon chain melting. This transition is similar to that described previously for numerous glycerol-based phospholipids, including PC (see, for example, refs. 30, 38–40). The chain melting transition, $T_m$, of C18 : 0-SM agrees with that reported recently by Cohen et al. [15] and Ahmad et al. [16], as does the transition enthalpy ($\Delta H = 6.7$ kcal/mol). Although $T_m$ is higher than that of C16 : 0-SM (Refs. 7, 14, 15, 16, 22), we have recently shown that the chain length dependence of $T_m$ and $\Delta H$ for an extensive series of SM (where only the *N*-acyl, and not the sphingosine chain, is changing) is more complex than that of a PC series where both *sn*-1 and *sn*-2 chains are altered [22] (see also Refs. 15 and 16).

For C18 : 0-SM, the hydration dependence of $T_m$ and

$\Delta H$ shows that $T_m$ decreases and $\Delta H$ increases with increasing hydration (see Fig. 3). This behavior is similar to that observed for C16:0-PC [38]. Our X-ray diffraction data of C18:0-SM at all hydration levels show a lamellar gel phase below the phase transition and lamellar liquid crystalline phase above the phase transition. The sharp, single wide-angle reflection ($1/4.2$ $Å^{-1}$) suggests that the hydrocarbon chains are arranged perpendicular to the bilayer plane and packed in a hexagonal array in the gel phase. From the combination of the gravimetric X-ray diffraction data and the derived electron density profiles, the hydration-dependence various structural parameters ($d$, $d_1$, $S$, and $d_{p\text{-}p}$) have been calculated (see Figs. 6a, 6b and 8). In the liquid crystalline phase, considering the assumptions implicit in the calculation of $d_1$, errors in the assumed value of $v_l$ and the limited resolution of the electron density profiles, a reasonably consistent picture of the hydration-dependence of the lipid thickness is obtained. $d_{p\text{-}p}$ ($\approx 41$ Å) is essentially independent of hydration and is close to $d_1$ values at hydration levels $> 20\%$. At hydration levels $< 20\%$, $d_1$ increases with decreasing hydration. The area per lipid molecule ($S$) increases from 38.5 Å² to 39 Å² up to approx. 20% hydration. This type of hydration-dependence of $d_1$, $d_{p\text{-}p}$ and $S$ has been observed for several other phospholipids in the liquid crystalline $L_\alpha$-phase (see, for example, dimyristoyl PC, see Ref. 30).

On the other hand, in the gel phase, over the hydration range 10–33% water, $d_{p\text{-}p}$ actually increases from 46 Å to 53 Å whereas $d_1$ decreases from 56 Å to 50.5 Å over a similar hydration range. As this stage it is not clear what combination of assumptions involved in the calculation of $d_1$, the invariant values of $v_l$ and $v_w$ used, and limited resolution of the electron density profiles is responsible for this apparent discrepancy. While $d_1$ and $d_{p\text{-}p}$ measure different parameters related to bilayer thickness (and thus different values of $d_1$ and $d_{p\text{-}p}$ might be expected), their opposite dependence on hydration below maximum hydration is puzzling. Interestingly, at and above maximum hydration there is quite good agreement between $d_1$ (51.5 Å) and $d_{p\text{-}p}$ (53.0 Å). The area ($S$) per SM molecule increases from 41 Å² to 45 Å² at the hydration limit. Otherwise, all the structural parameters indicate the presence of conventional gel and liquid crystalline bilayer phases.

Our DSC and X-ray diffraction data show that C18:0-SM has a well defined bilayer structure at all hydration levels in both the gel and liquid crystalline phases. An order-disorder transition separates the high temperature liquid crystalline phase from a more ordered gel phase at low temperature. In the absence of water, a transition occurs at 75°C. Addition of water between adjacent bilayers progressively lowers the transition temperature to a limiting value of approx. 45°C. In the gel phase at 22°C, the C18:0-SM bilayer shows a maximum water uptake of 31.5%. Above this water content, the maximally swollen lamellar lipid phase coexists with an excess bulk water phase. In the liquid crystalline phase at 55°C, the hydration limit is 35% water. The low enthalpy transition ($\Delta H = 0.6$ kcal/mol) of C18:0-SM at lower hydrations is probably due to the formation of a low temperature sub-gel phase analogous to that observed for dipalmitoyl-PC [41–44], but this remains to be established.

The present study has provided detailed structural and thermodynamic information on hydrated C18:0-SM. In contrast to natural sphingomyelins [6,8,12], C18:0-SM contains a well defined amide-linked fatty acid chain, C18:0, similar in length to the C18 sphingosine chain. However, due to the location of the amide bond at C2 of sphingosine and the conformation around C2 [45,46], a small mismatch in the two chains at the layer center may occur. SM with 'well-matched' chains (e.g., C16:0- and C18:0-SM) exhibit simple bilayer thermotropic properties, whereas when the N-linked chain is either shorter (C14:0-SM) or longer (C24:0-SM) more complex thermotropic behavior is observed [22,23].

In contrast to the simple behavior of C18:0-SM observed here, Estep et al. [17] showed that fully hydrated DL-*erythro* C18:0-SM exhibits more complex behavior. A 'crystalline chain' bilayer gel phase converts to a bilayer liquid crystalline $L_\alpha$ phase at 57°C, accompanied by a high enthalpy change (20 kcal/mol). On cooling from the $L_\alpha$ phase, marked supercooling occurs with conversion to a metastable bilayer gel phase at approx. 44°C. Reversible transitions between the metastable bilayer gel phase and the $L_\alpha$ phase occur at 45°C with a lower transition enthalpy ($\approx 7$ kcal/mol). This latter reversible behavior of DL-*erythro* C18:0-SM is very similar to that observed for the partially-synthetic C18:0-SM studied here. Recently, Bruzik and Tsai [47] described the de novo synthesis of chemically and stereochemically pure C18:0-SM. While the reversible DSC behavior of both D-*erythro*- and L-*threo* C18:0-SM [47] is similar to that described here for partially-synthetic C18:0-SM ($T_m \approx 45$°C; $\Delta H = 6.5$–$7.5$ kcal/mol), marked differences in the stability of the gel phases is observed. In particular, Bruzik and Tsai [47] provide convincing evidence for the formation of multiple low-temperature gel phases following low-temperature incubation. Thus, as might be expected, the totally synthetic DL-*erythro* [17], D-*erythro* and L-*threo* [47] SM exhibit more complex polymorphic behavior in the gel phase than does the partially-synthetic C18:0-SM studied here, or indeed the previously studied bovine brain SM [6]. The interaction of cholesterol with C18:0-SM [48], the structure and properties of C16:0-SM and its interaction with cholesterol and dipalmitoyl-PC [49], and the structure and properties of C24:0-SM [50] will be described in future publications.

**Acknowledgements**

We thank David Jackson for technical help and Dr. David Atkinson for helpful advice. We thank Irene Miller for help in preparing the manuscript. This research was supported by Research Grant HL-26335 and Training Grant HL-07291 from the National Institutes of Health.

**References**

1 Barenholz, Y. and Thompson, T.E. (1980) Biochim. Biophys. Acta 604, 129–158.
2 Barenholz, Y. and Gatt, S. (1982) in Phospholipids (Hawthorne, J.N. and Ansell, G.B., eds.), pp. 129–177, Elsevier Biomedical Press, Amsterdam.
3 Shah, D.O. and Schulman, J.H. (1967) Lipids 2, 21–27.
4 Shah, D.O. and Schulman, J.H. (1967) Biochim. Biophys. Acta 135, 184–187.
5 Reiss-Husson, F. (1967) J. Mol. Biol. 25, 363–382.
6 Shipley, G.G., Avecilla, L.S. and Small, D.M. (1974) J. Lipid Res. 15, 124–131.
7 Barenholz, Y., Suurkuusk, J., Mountcastle, D., Thompson, T.E. and Biltonen, R.L. (1976) Biochemistry 15, 2441–2447.
8 Untracht, S.H. and Shipley, G.G. (1977) J. Biol. Chem. 252, [illegible]–4457
9 Oldfield, E. and Chapman [illegible] FEBS Lett. 21, 303–306.
10 Long, R.A., Hruska, F.E., Gesser, H.D. and Hsia, J.C. (1971) Biochem. Biophys. Res. Commun. 45, 167–173.
11 Khare, R.S. and Worthington, C.R. (1977) Mol. Cryst. Liq. Cryst. 38, 195–206.
12 Calhoun, W.I. and Shipley, G.G. (1979) Biochim. Biophys. Acta 555, 436–441.
13 Shapiro, D. and Flowers, H.M. (1962) J. Am. Chem. Soc. 84, 1047–1050.
14 Calhoun, W.I. and Shipley, G.G. (1979) Biochemistry 18, 1717–1722.
15 Cohen, R., Barenholz, Y., Gatt, S. and Dagan, A. (1984) Chem. Phys. Lipids 35, 371–384.
16 Ahmad, T.Y., Sparrow, J.T. and Morrisett, J.D. (1985) J. Lipid Res. 26, 1160–1165.
17 Estep, T.N., Calhoun, W.I., Barenholz, Y., Biltonen, R.L., Shipley, G.G. and Thompson, T.E. (1980) Biochemistry 19, 20–24.
18 Estep, T.N., Mountcastle, D.B., Barenholz, Y., Biltonen, R.L. and Thompson, T.E. (1979) Biochemistry 18, 2112–2117.
19 Estep, T.N., Freire, E., Anthony, F., Barenholz, Y., Biltonen, R.L. and Thompson, T.E. (1981) Biochemistry 20, 7115–7118.
20 Lentz, B.R., Hoechli, M. and Barenholz, Y. (1981) Biochemistry 20, 6803–6809.
21 Demel, R.A., Jansen, J.W.C.M., Van Dijck, P.W.M. and Van Deenen, L.L.M. (1977) Biochim. Biophys. Acta 465, 1–10.
22 Sripada, P.K., Maulik, P.R., Hamilton, J.A. and Shipley, G.G. (1987) J. Lipid Res. 28, 710–718.
23 Maulik, P.R., Atkinson, D. and Shipley, G.G. (1986) Biophys. J. 50, 1071–1077.
24 Kaller, H. (1961) Biochem. Z. 334, 451–456.
25 Elliott, A.J. (1965) J. Sci. Instrum. 42, 312–316.
26 Franks, A. (1958) Br. J. Appl. Phys. 9, 349–352.
27 Luzzati, V. (1968) in Biological Membranes (Chapman, D., ed.), pp. 71–123, Academic Press, London and New York.
28 Nagle, J.F. and Wilkinson, D.A. (1978) Biophys. J. 23, 159–175.
29 Torbet, J. and Wilkins, M.H.F. (1976) J. Theor. Biol. 62, 447–458.
30 Janiak, M.J., Small, D.M. and Shipley, G.G. (1979) J. Biol. Chem. 254, 6068–6078.
31 McDaniel, R.V., McIntosh, T.J. and Simon, S.A. (1983) Biochim. Biophys. Acta 731, 97–108.
32 Mattai, J. and Shipley, G.G. (1986) Biochim. Biophys. Acta 859, 257–265.
33 McIntosh, T.J. and Simon, S.A. (1986) Biochemistry 25, 4058–4066.
34 Shah, J., Sripada, P.K. and Shipley, G.G. (1990) Biochemistry 29, 4254–4262
35 Worthington, C.R. and Blaurock, A.E. (1969) Biophys. J. 9, 970–990.
36 Shannon, C.E. (1949) Proc. Inst. Radio. Eng. NY, 37, 10–21.
37 King, G.I. and Worthington, C.R. (1971) Phys. Lett. A35, 259–260.
38 Chapman, D., Williams, R.M. and Ladbrooke, B.D. (1967) Chem. Phys. Lipids 1, 445–475.
39 Tardieu, A., Luzzati, V. and Reman, F.C. (1973) J. Mol. Biol. 75, 711–733.
40 Janiak, M.J., Small, D.M. and Shipley, G.G. (1976) Biochemistry 15, 4575–4580.
41 Chen, S.C., Sturtevant, J.M. and Gaffney, B.J. (1980) Proc. Natl. Acad. Sci. USA 77, 5060–5063.
42 Füldner, H.H. (1981) Biochemistry 20, 5707–5710.
43 Ruocco, M.J. and Shipley, G.G. (1982) Biochim. Biophys. Acta 684, 59–66.
44 Ruocco, M.J. and Shipley, G.G. (1982) Biochim. Biophys. Acta 691, 309–320.
45 Sundaralingam, M. (1972) Ann. N.Y. Acad. Sci. 195, 324–355.
46 Bruzik, K.S. (1988) Biochim. Biophys. Acta 939, 315–326.
47 Bruzik, K.S. and Tsai, M.-D. (1987) Biochemistry 26, 5364–5368.
48 Maulik, P.R., Sripada, P.K. and Shipley, G.G. (1985) Biophys. J. 47, 44a.
49 Maulik, P.R., Sripada, P.K. and Shipley, G.G. (1986) Biophys. J. 49, 505a.
50 Maulik, P.R. and Shipley, G.G., in preparation.